

Research Journal of Pharmaceutical, Biological and Chemical Sciences

Evaluation of Cytotoxic, Antioxidant And Antimicrobial Activities of (E)-N`-(1-(pyridine-2-yl)ethylidene)benzohydrazide Complexes.

O K Al-Duaij*.

Department of Chemistry, Science College, Al Imam Mohammad Ibn Saud Islamic University, (IMSIU), Riyadh, KSA, P.O. Box 90950, Riyadh 11623, Saudi Arabia.

ABSTRACT

(E)-N`-(1-(pyridine-2-yl)ethylidene)benzohydrazide (HL) and its Ni(II), Cu(II), Pd(II), Cd(II), Hg(II) and UO₂(II) complexes have been prepared. The complex structures were elucidated by using analysis (elemental and thermal), spectroscopy (UV-visible, IR, ESR, ¹H and ¹³C-NMR spectra) and physical measurements (magnetic susceptibility and molar conductance). The semi-empirical method PM3, ¹H NMR, ¹³C-NMR and IR spectra indicated that the ligand acts as bidentate and/or tridentate ligand. The room temperature solid state ESR spectra of the Cu(II) complexes show $d_{x^2-y^2}$ as a ground state, suggesting square planer geometry around Cu(II) center. The bond length, bond angle, HOMO, LUMO and dipole moment have been calculated to confirm the geometry of the ligand and its complexes. Also, the interpretation, mathematical analysis and evaluation of kinetic and thermodynamic parameters of all thermal decomposition steps were evaluated using Coats–Redfern and Horowitz-Metzger methods. Moreover, antimicrobial activity of ligand and its complexes were studied against gram-negative bacteria: Escherichia coli and pathogenic fungi Candida albicans by using minimum inhibitory concentrations (MICs) method. Compounds **4** and **5** show the best activity while compound **6** was the best antioxidant reagents using the DPPH method. Finally, the compounds were also screened for cytotoxicity study against Ehrlich ascites cells. Compounds **3**, **4** and **6** showed very high cytotoxicity in comparison with standard drug 5-FU.

Keywords: Cytotoxic activity; Antioxidant activity; Antimicrobial activity; Molecular modeling; PM3 calculations.

*Corresponding author

INTRODUCTION

Diseases caused by microbial infections are a hard attack to the health of human being and often have a connection to some different diseases whenever the body system gets debilitated [1-3]. Developing antimicrobial drugs and keeping their potency in opposition to resistance by using different types of microorganisms as a broad spectrum of antibacterial activity are some of the major concerns of research in this area [4-6]. In recent years, there has been an interest in the application of antioxidants to medical treatment as information is constantly gathered linking the development of human diseases to oxidative stress. Also, free radicals play an important role in the pathogenesis of chronic degenerative diseases including cancer, inflammatory, cardiovascular and neurodegenerative diseases [7-9]. Moreover, it is known that oxidative stress can be induced by a wide range of environmental factors including UV stress, pathogen invasion, herbicide action and oxygen shortage [10]. Based on these facts, synthetic and natural compounds with potential antioxidant activity are receiving increased attention in biological studies, medicine and pharmacy [11].

In continuing search for potent and selective cytotoxic antitumor agents, [12, 13] we synthesized and characterized (E)-N`-(1-(pyridine-2-yl)ethylidene) benzohydrazide (HL) and its metal complexes of Ni(II), Cu(II), Pd(II), Cd(II), Hg(II) and UO₂(II). The antioxidant, antimicrobial and cytotoxic activities of the isolated compounds were evaluated.

EXPERIMENT PROTOCOLS

Synthesis of ligand HL

The ligand (E)-N-(1-(pyridine-2-yl)ethylidene)benzohydrazide (HL) was prepared by heating a mixture of benzohydrazide (0.01 mol; 1.36 g) and 2-acetylpyridine (0.01 mol; 3.06 g) under reflux in absolute ethanol for 3 h. (Scheme 1). On heating, white crystals were formed, filtered off, washed with absolute ethanol and diethyl ether and recrystallized from EtOH. The purity of the compound was checked by TLC.

4.1.1 HL, **(1)**. Found (white crystal): C, 70.2; H, 5.5; Calc. (for C₁₄H₁₃N₃O): C, 70.3; H, 5.5%. Yield: 90%, m.p. 125 °C. IR (KBr, cm⁻¹, ν(NH) 3233; ν(C=O) 1685; (C=N)_{azo} 1661; (C=N)_{py} 631. NMR (¹H, DMSO-d₆, ppm, s: singlet, d: doublet, m: multiplet): 10.81 (s, 1H, NH); 2.60 (s, 3H, CH₃); 8.22 (d, 1H, H³); 7.91 (t, 2H, H⁴); 7.47 (t, 1H, H⁵); 8.64 (d, 1H, H⁶); 8.58 (d, 2H, H^{11, 13}); 8.38 (d, 2H, H^{10, 14}). NMR (¹³C, DMSO-d₆, ppm): δ 149.14 (C²); 120.33 (C³); 136.61 (C⁴); 124.25 (C⁵); 134.57 (C⁶); 154.76 (C⁷); 162.68 (C⁸); 134.16 (C⁹); 139.61 (C¹²); 129.52 (C^{10, 14}); 123.30 (C^{11, 13}).

Synthesis of metal complexes

The complexes were prepared by mixing equimolar amounts of HL with ethanolic and/or aqueous solution of chloride salt of Cu(II), Cd(II) Hg(II) and Pd(II) as potassium tetrachloropalladate; acetate salt of Ni(II) and UO₂(II). The reaction mixture was heated under reflux on a water bath for 1–3 h. The precipitate was filtered off, washed with hot EtOH and/or H₂O successfully and finally preserved in a vacuum desiccator over anhydrous CaCl₂. The complexes are powder-like, stable in the normal laboratory atmosphere, and soluble in DMF or DMSO. The characterization of these complexes was based on the physical and spectroscopic techniques.

[Ni(L)₂], **(2)**. Found (red): C, 62.9; H, 4.6; Ni, 10.9% Calc. (for PdC₂₈H₂₆N₆O₂Cl₂): C, 62.8; H, 4.5; Ni, 11.0% Yield:

80%, m.p. >300 °C. IR (KBr, cm⁻¹, ν(NH) disappear; ν(C=O) disappear; ν(C=N*) 1635; ν(C-O)_{enolic} 1142; (C=N)_{azo} 1600; (C=N)_{py} 626, ν(M—O) 533; ν(M—N) 429. NMR (¹H, DMSO-d₆, ppm, s: singlet, d: doublet, m: multiplet): (NH, disappear); 2.60 (s, 3H, CH₃); 8.18 (d, 1H, H³); 8.22 (t, 2H, H⁴); 7.75 (t, 1H, H⁵); 8.60 (d, 1H, H⁶); 7.46 (d, 2H, H^{11, 13}); 8.30 (d, 2H, H^{10, 14}). NMR (¹³C, DMSO-d₆, ppm): δ 146.54 (C²); 125.63 (C³); 140.87 (C⁴); 127.35 (C⁵); 139.50 (C⁶); 159.86 (C⁷); 172.08 (C⁸); 139.18 (C⁹); 139.90 (C¹²); 130.24 (C^{10, 14}); 123.20 (C^{11, 13}).

[Hg(HL)₂Cl₂], **(3)**. Found (yellowish-white): C, 44.7; H, 3.5; Hg, 26.7; Cl, 9.5% Calc. (for HgC₂₈H₂₆N₆O₂Cl₂): C, 44.8; H, 3.5; Hg, 26.7; Cl, 9.4% Yield: 85%, m.p. >300 °C. IR (KBr, cm⁻¹, ν(NH) 3264; ν(C=O) 1654; (C=N)_{azo} 1610; (C=N)_{py} 625, ν(M—O) 545; ν(M—N) 460. NMR (¹H, DMSO-d₆, ppm, s: singlet, d: doublet, m:

multiplet): 10.87 (s, 1H, NH); 2.57 (s, 3H, CH₃); 8.16 (d, 1H, H³); 8.20 (t, 2H, H⁴); 7.71 (t, 1H, H⁵); 8.62 (d, 1H, H⁶); 7.49 (d, 2H, H^{11, 13}); 8.32 (d, 2H, H^{10, 14}). NMR (¹³C, DMSO-d₆, ppm): δ 148.36 (C²); 125.31 (C³); 140.56 (C⁴); 127.40 (C⁵); 139.53 (C⁶); 150.46 (C⁷); 170.08 (C⁸); 138.15 (C⁹); 139.90 (C¹²); 129.45 (C^{10, 14}); 123.28 (C^{11, 13}).

[Cd(HL)₂Cl₂], (**4**). Found (white): C, 50.7; H, 4.0; Cd, 16.9; Cl, 10.8% Calc. (for CdC₂₈H₂₆N₆O₂Cl₂): C, 50.8; H, 3.9; Cd, 17.0; Cl, 10.7% Yield: 85%, m.p. >300 °C. IR (KBr, cm⁻¹, ν(NH) 3208; ν(C=O) 1654; (C=N)_{azo} 1612; (C=N)_{py} 616; ν(M—O) 531; ν(M—N) 445. NMR (¹H, DMSO-d₆, ppm, s: singlet, d: doublet, m: multiplet): 10.87 (s, 1H, NH); 2.57 (s, 3H, CH₃); 8.16 (d, 1H, H³); 8.20 (t, 2H, H⁴); 7.71 (t, 1H, H⁵); 8.62 (d, 1H, H⁶); 7.49 (d, 2H, H^{11, 13}); 8.32 (d, 2H, H^{10, 14}). NMR (¹³C, DMSO-d₆, ppm): δ 148.34 (C²); 125.33 (C³); 140.57 (C⁴); 127.37 (C⁵); 139.53 (C⁶); 152.96 (C⁷); 170.16 (C⁸); 138.11 (C⁹); 139.93 (C¹²); 129.55 (C^{10, 14}); 123.24 (C^{11, 13}).

[Cu(L)Cl], (**5**). Found (green): C, 40.1; H, 5.9; Cu, 12.9; Cl, 10.5% Calc. (for CuC₁₄H₁₂N₃OCl): C, 40.1; H, 5.8; Cu, 13.1; Cl, 10.5% Yield: 70%, m.p. 270 °C. IR (KBr, cm⁻¹, ν(NH) disappear; ν(C=O) disappear; ν(C=N*) 1640; ν(C—O)_{enolic} 1176; (C=N)_{azo} 1613; (C=N)_{py} 643, ν(M—O) 560; ν(M—N) 445.

[Pd(HL)₂Cl₂], (**6**). Found (yellow): C, 51.3; H, 4.0; Pd, 16.3; Cl, 10.7% Calc. (for PdC₂₈H₂₆N₆O₂Cl₂): C, 51.3; H, 3.9; Pd, 16.2; Cl, 10.8% Yield: 88%, m.p. >300 °C. IR (KBr, cm⁻¹, ν(NH) 3245; ν(C=O) 1694; (C=N)_{azo} 1615; (C=N)_{py} 658, ν(M—O) 525; ν(M—N) 420. NMR (¹H, DMSO-d₆, ppm, s: singlet, d: doublet, m: multiplet): 10.87 (s, 1H, NH); 2.57 (s, 3H, CH₃); 8.16 (d, 1H, H³); 8.20 (t, 2H, H⁴); 7.71 (t, 1H, H⁵); 8.62 (d, 1H, H⁶); 7.49 (d, 2H, H^{11, 13}); 8.32 (d, 2H, H^{10, 14}). NMR (¹³C, DMSO-d₆, ppm): δ 146.34 (C²); 125.33 (C³); 140.57 (C⁴); 127.37 (C⁵); 139.53 (C⁶); 150.96 (C⁷); 165.68 (C⁸); 138.11 (C⁹); 139.93 (C¹²); 129.55 (C^{10, 14}); 123.24 (C^{11, 13}).

[UO₂(L)(OAc)(H₂O)], (**7**). Found (red): C, 33.0; H, 3.0; U, 40.7% Calc. (for UC₁₆H₁₇N₃O₆): C, 32.8; H, 2.9; U, 40.6% Yield: 86%, m.p. >300 °C. IR (KBr, cm⁻¹, ν(NH) disappear; ν(C=O) disappear; ν(C=N*) 1638; ν(C—O)_{enolic} 1164; (C=N)_{azo} 1615; (C=N)_{py} 640, ν(M—O) 557; ν(M—N) 452. NMR (¹H, DMSO-d₆, ppm, s: singlet, d: doublet, m: multiplet): (NH, disappear); 2.59 (s, 3H, CH₃); 8.14 (d, 1H, H³); 8.22 (t, 2H, H⁴); 7.75 (t, 1H, H⁵); 8.60 (d, 1H, H⁶); 7.52 (d, 2H, H^{11, 13}); 8.22 (d, 2H, H^{10, 14}). NMR (¹³C, DMSO-d₆, ppm): δ 146.54 (C²); 125.39 (C³); 140.62 (C⁴); 127.39 (C⁵); 139.51 (C⁶); 158.94 (C⁷); 171.44 (C⁸); 138.11 (C⁹); 139.93 (C¹²); 130.15 (C^{10, 14}); 123.24 (C^{11, 13}).

Analyses of the complexes

Elemental analyses

The complexes were analyzed for metal content gravimetrically by literature procedures [52] after decomposing the organic matter with a mixture of HNO₃ and HCl and evaporating the residue to dryness with concentrated H₂SO₄. Carbon and hydrogen were determined microanalytically at the Microanalytical Unit of Cairo University.

Physico-chemical measurements

The molar conductance of the complexes were determined by preparing 10⁻³ M solutions of the complexes in DMSO at room temperature and measured on an YSI Model 32 conductivity bridge. Thermogravimetric analysis was performed using an automatic recording thermobalance type (DuPont 951 instrument).

Molecular modeling

An attempt to gain a better insight on the molecular structure of the ligand and its complexes, geometry optimization and conformational analysis has been performed by the use of MM+ force-field as implemented in hyperchem 8.03 [22]. The low lying obtained from MM+ [53] was then optimized at PM3 using the Polak-Ribiere algorithm in RHF-SCF, set to terminate at an RMS gradient of 0.01 kcal mol⁻¹. Energy minima for **1**, **2**, **4**, **5**, **6** and **7** were determined by a semi-empirical method PM3 (as implemented in HyperChem 8.03). The conformations thus obtained were confirmed as minima by vibrational analysis. Atom-centred charges for each molecule were computed from the PM3 wavefunctions (HyperChem 8.03) which provides derived charges that closely resemble those obtainable from ab initio 6-31G* calculations.

Antimicrobial activity

The compounds, Gentamycin and Colitrimazole were dissolved in DMSO at concentration of 1µg/ml. The twofold dilutions of the solution were prepared. The microorganism suspensions [54] at 10CFU/ml (colony forming unit/ml) concentration were inoculated to the corresponding wells. The plates were incubated at 36 °C for 24 and 48h for the bacteria and *C. albicans*, respectively. The MIC values were determined as the lowest concentration that completely inhibited visible growth of the microorganism as detected by unaided eye.

4.6. Evaluation of the cytotoxicity of the synthesized compounds

To examine whether the synthesized compounds have a direct cytotoxic effect on Ehrlich ascites cells (EAC), viability, the percentage of viable cells was estimated by the trypan blue [55] exclusion test. The desired concentration of tumor cells (2×10^6 cells per 0.2 ml) was obtained by dilution with saline solution (0.9% sodium chloride). Viability of tumor cells obtained and used in this experiment was always higher than 90%. Below this percentage, the cells were discarded and the entire procedure was repeated.

Antioxidant activity

The hydrogen atom or electron donation ability of the corresponding compounds was measured from the bleaching of purple colored of methanolic solution of DPPH. This spectrophotometric assay uses stable radical diphenylpicrylhydrazyl (DPPH) as a reagent [56,57]. Stock solution (1 mg/mL) was diluted to final concentrations of 20–100 µg/mL. Different concentrations of the chemical compounds were dissolved in methanol to obtain final concentration ranged from 6.25 to 100 mg/mL different concentrations were made to determine IC_{50} (concentration make 50% inhibition of DPPH color). Fifty microliters of various sample concentrations were added to 5 mL of 0.004% methanolic solution of DPPH. After a 60 min of incubation at dark the mixture was shaken vigorously and allowed to stand at room temperature, the absorbance was read against a blank at 517 nm. Inhibition free radical DPPH in percent (I %) was calculated as in Eq :

$$I\% = (A_{\text{blank}} - A_{\text{sample}}) / (A_{\text{blank}}) \times 100$$

Where A_0 is the absorbance of the control reaction and A_1 is the absorbance in the presence of the samples or standards.

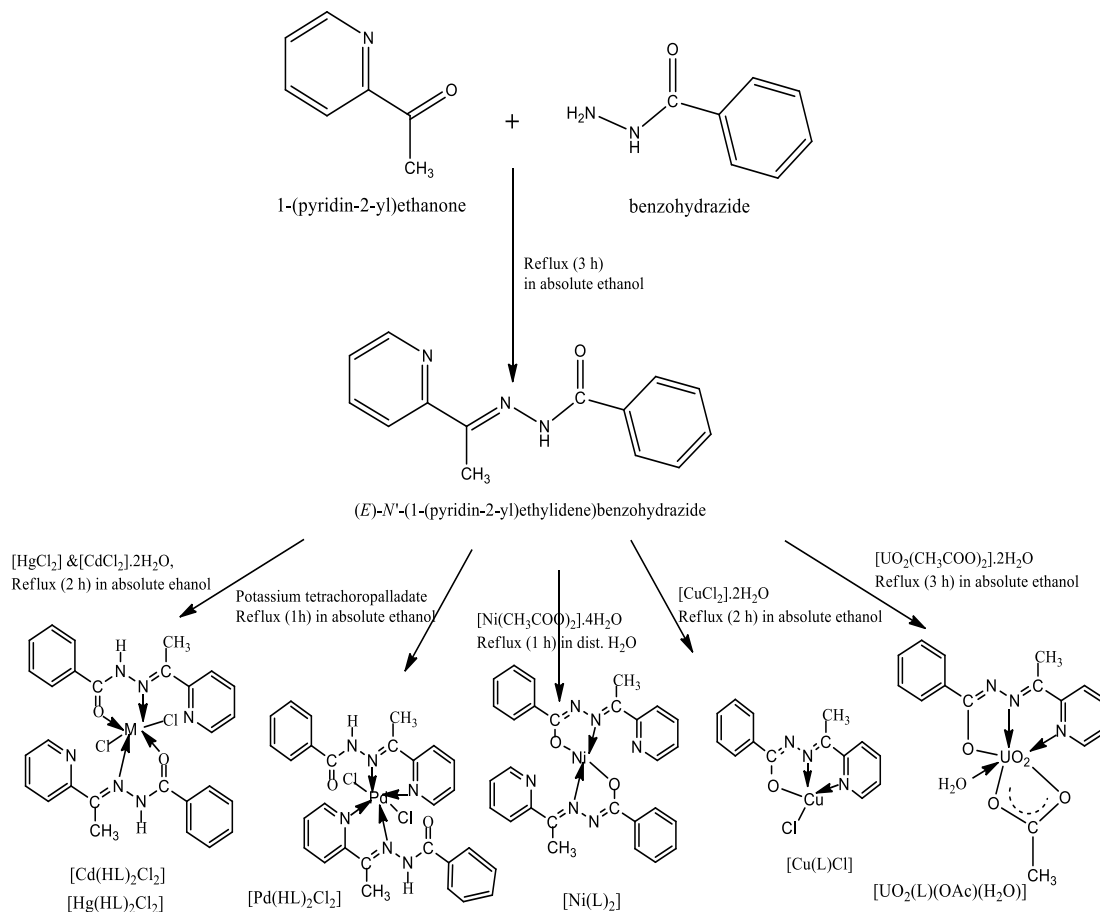
Antioxidant activity screening assay for erythrocyte hemolysis.

The hemolytic activity of the synthesized ligand and its metal complexes were determined using Wister rat erythrocytes. The RBCs were prepared as follows: 2–3 ml of rat blood was drawn into 12 ml of heparinized 5 mM HEPES buffer pH 7.4 containing 150 mM NaCl and centrifuged at 4000 rpm for 5 min. Erythrocytes were separated from plasma and the buffy coat was washed three times with 10 volumes of 0.15 M NaCl. Working stocks of RBCs were made by diluting the RBCs pellet (0.5–0.8 ml) to about 15 ml with buffer. For standardization of the volume for lysis assay, different volumes (5–40 µl) of diluted blood samples were drawn into 1 ml of water containing 0.1% of Triton X-100 and buffer with RBCs was used as blank. The solution was centrifuged at 4000 rpm. The absorbance of the supernatant was read at 540 nm. The volume of RBCs was standardized so as the absorbance was about ~0.2 OD (about 2×10^6 cells/ml) range. This suitable volume was used for the hemolysis assay with synthesized compounds. Different volumes of compounds were taken in 1.5 ml eppendorf tubes containing 5 mM HEPES buffer pH 7.4 containing 150 mM NaCl. To this, diluted blood suspension (volume as determined above) was added and total volume in the reaction tube was made up to 1 ml with buffer. The tubes were incubated at 37 °C for 30 min in a gentle shaking water bath.

After incubation, the samples were centrifuged in a Kubota centrifuge at 4000 rpm for 5 min to remove the unhemolysed cells. Similarly, the reaction mixture was treated with 8 volumes of distilled water to achieve complete hemolysis, and the absorbance of the supernatant obtained after centrifugation was measured at 540 nm. The data percentage hemolysis was expressed as mean \pm standard deviation. L-ascorbic acid was used as a positive control.

RESULTS AND DISCUSSION

The ligand and its complexes (Scheme 1) are stable under normal conditions of temperature and pressure. The ligand is soluble in common organic solvents but its complexes are soluble in DMF and DMSO. Elemental analysis of the ligand and its complexes are in agreement with the presented formula. Molar conductivity values indicate that complexes are non-electrolytes.



Scheme 1: The outline of the synthesis of ligand and its complexes.

IR spectral studies

The infrared spectrum of HL displays four important bands at 1685, 1661, 631 and 3233 cm^{-1} assigned to $\nu(\text{C}=\text{O})$ [14], $\nu(\text{C}=\text{N})_{\text{hydrazone}}$ [15], $\nu(\text{C}=\text{N})_{\text{py}}$ [16] and $\nu(\text{NH})$ [17] vibrations, respectively.

Comparison of the infrared spectrum of the ligand with those of its metal complexes reveals that HL (Structure 1) behaves as a bidentate and/or tridentate ligand depending on the metal salt and the reaction conditions.

In $[\text{Cd}(\text{HL})_2\text{Cl}_2]$ (Structure 2) and $[\text{Hg}(\text{HL})_2\text{Cl}_2]$ complexes, HL acts as a neutral bidentate ligand coordinating via carbonyl oxygen ($\text{C}=\text{O}$) and azomethine nitrogen ($\text{C}=\text{N})_{\text{hydrazone}}$. This mode of chelation is supported by the shift of both $\nu(\text{C}=\text{N})$ and $\nu(\text{C}=\text{O})$ vibrations to lower wavenumber. The $\nu(\text{NH})$ vibration remains more or less at the same position. Also, the infrared spectra of these complexes show new bands at (531, 249) and (445, 460) cm^{-1} which assignable to $\nu(\text{M}-\text{O})$ and $\nu(\text{M}-\text{N})$, respectively.

Also, in $[\text{Pd}(\text{HL})_2\text{Cl}_2]$ complex (Structure 3), HL acts as a neutral bidentate ligand coordinating via azomethine nitrogen ($\text{C}=\text{N})_{\text{hydrazone}}$ and pyridyl nitrogen ($\text{C}=\text{N})_{\text{py}}$. This mode of coordination is supported by the shift of both $\nu(\text{C}=\text{N})_{\text{hydrazone}}$ and $\nu(\text{C}=\text{N})_{\text{py}}$ vibrations to lower wavenumber. The $\nu(\text{C}=\text{O})$ and $\nu(\text{NH})$ vibrations shift

to higher wavenumber. Also, the infrared spectrum of this complex shows new bands at 542 and 422 cm^{-1} which assignable to $\nu(\text{Pd}-\text{O})$ and $\nu(\text{Pd}-\text{N})$, respectively.

Moreover, in $[\text{Ni}(\text{L})_2]$ complex (Structure 4), HL acts as a mononegative bidentate ligand coordinating via the azomethine nitrogen ($\text{C}=\text{N}$)_{hydrazone} and the deprotonated enolized carbonyl group forming two five membered rings including the metal atom. This mode of complexation is supported by the disappearance of both $\nu(\text{C}=\text{O})$ and $\nu(\text{NH})$ with simultaneous appearance of new bands at 1635 and 1142 cm^{-1} assignable to $\nu(\text{C}=\text{N}^*)$ and $\nu(\text{C}-\text{O})$ _{enolic} [18]; the negative shift of $\nu(\text{C}=\text{N})$ _{hydrazone} and the appearance of new bands at 533 and 429 cm^{-1} assigned to $\nu(\text{Ni}-\text{O})$ and $\nu(\text{Ni}-\text{N})$, respectively.

Finally, HL behaves as a mononegative tridentate ligand coordinating through the pyridyl nitrogen ($\text{C}=\text{N}$)_{py}, azomethine nitrogen ($\text{C}=\text{N}$) and deprotonated enolized carbonyl oxygen ($=\text{C}-\text{O}^-$). This behaviour is observed in $[\text{Cu}(\text{L})\text{Cl}]$ (Structure 5) and $[\text{UO}_2(\text{L})(\text{OAc})(\text{H}_2\text{O})]$ complexes. This mode of chelation is based on the disappearance of both $\nu(\text{C}=\text{O})$ and $\nu(\text{NH})$ with simultaneous appearance of new band at (1638, 1640) and (1164, 1176) cm^{-1} assignable to $\nu(\text{C}=\text{N}^*)$ and $\nu(\text{C}-\text{O})$ _{enolic}; the negative shift of $\nu(\text{C}=\text{N})$; the positive shift of $\nu(\text{C}=\text{N})$ _{py} and the appearance of new bands at (557, 560) and (445, 452) cm^{-1} attributed to $\nu(\text{M}-\text{O})$ and $\nu(\text{M}-\text{N})$, respectively. Also, the $[\text{UO}_2(\text{L})(\text{OAc})(\text{H}_2\text{O})]$ complex (Structure 6) shows two bands at 1466 and 1559 cm^{-1} attributable to the $\nu_s(\text{O}-\text{C}-\text{O})$ and $\nu_{as}(\text{O}-\text{C}-\text{O})$ of the acetate group. The difference (93 cm^{-1}) between those two bands indicating the bidentate character for the acetate group [19]. In addition this complex has coordinated water molecule which indicated by two bands at 860 and 778 cm^{-1} assignable to $\rho_r(\text{H}_2\text{O})$ [19] and $\rho_w(\text{H}_2\text{O})$ [19] vibrations, respectively. Moreover, strong evidence for the presence or absence of water of crystallization and/or coordinated water supported by the thermogram of all complexes.

The IR spectrum of $[\text{UO}_2(\text{L})(\text{OAc})(\text{H}_2\text{O})]$ complex displays two bands at 923 and 870 cm^{-1} assigned to ν_3 and ν_1 vibrations, respectively, of the dioxouranium ion. The ν_3 value is used to calculate the force constant (F) of $\nu(\text{U}=\text{O})$ by the method of McGlynn et al [20]

$$(\nu_3)^2 = (1307)^2 (F_{\text{U-O}})/14.103$$

The force constant obtained for uranyl complex was then substituted into the relation given by Jones [21]

$$R_{\text{U-O}} = 1.08 (F_{\text{U-O}})^{-1/4} + 1.17$$

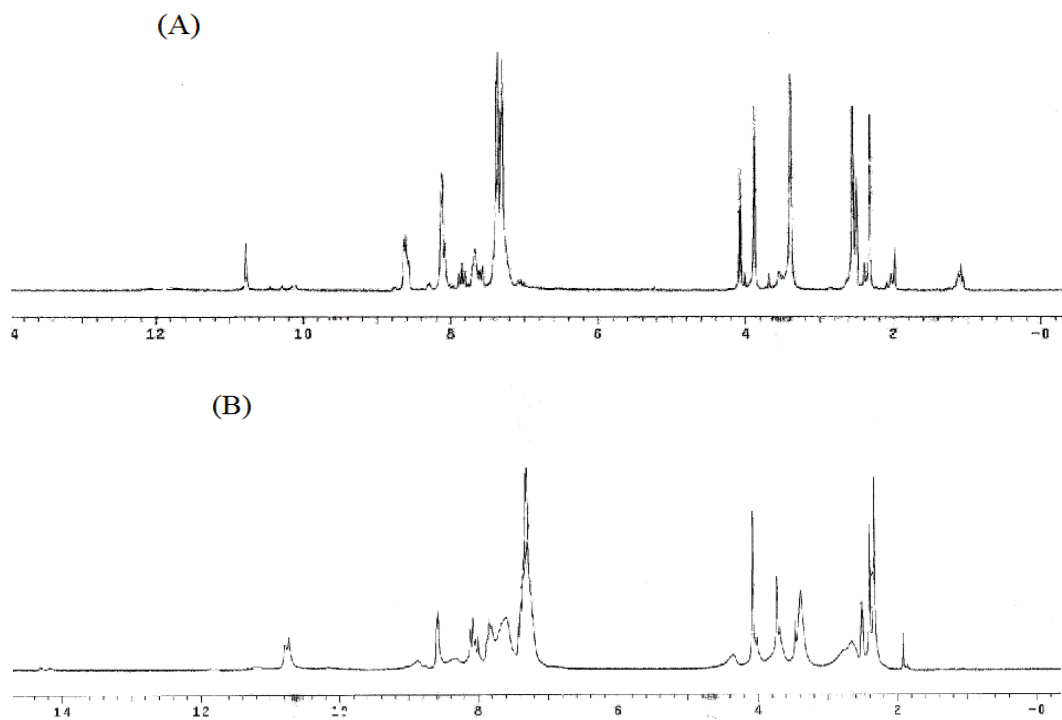
To give an estimate of the (U-O) bond length in Å. The calculated $F_{\text{U-O}}$ and $R_{\text{U-O}}$ values are 7.033 $\text{mdynes } \text{Å}^{-1}$ and 1.734 Å, respectively, fall in the usual range for the uranyl complexes [21]. The U-O bond distance falls in usual region as reported earlier [14] and extremely is consistent with the bond length calculated by the use of MM+ force field (as implemented in hyperchem 8.03) [22].

Nuclear magnetic resonance spectral studies

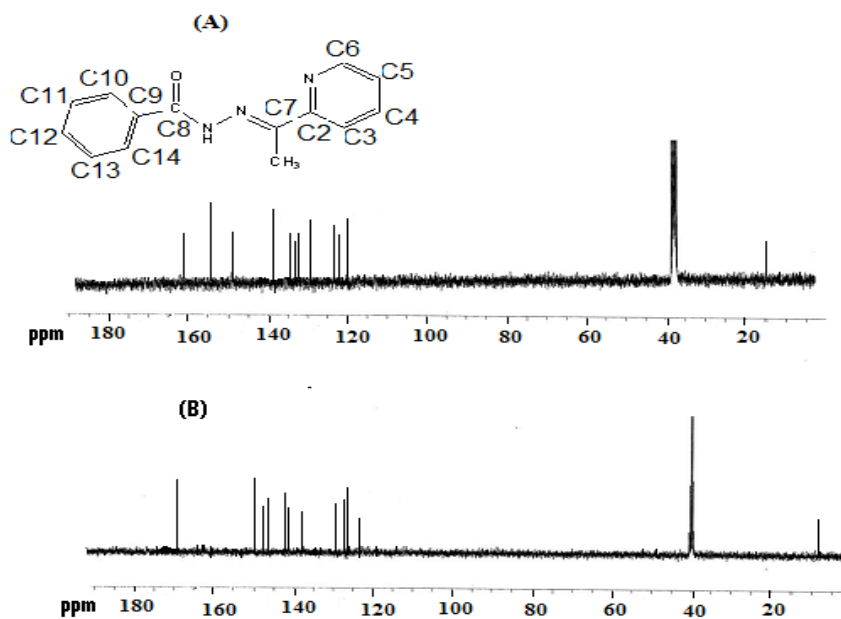
The ^1H and ^{13}C NMR spectra of HL and its diamagnetic complexes (Schemes 2, 3) were recorded in DMSO. The ^1H NMR spectrum of HL in DMSO shows one signal at 10.81 ppm assignable to the proton of (NH). The multiplet signals observed in the 7.47-8.64 ppm region are assigned to the aromatic protons. The sharp singlet observed at 2.6 ppm is assigned to methyl protons ($-\text{N}=\text{C}-\text{CH}_3$). Also, the ^1H NMR spectra of the Cd(II), Pd(II) and Hg(II) complexes show the signals attributed to the NH proton remain more or less at the same positions indicating that these groups play no part in coordination. But, the lack of signal of NH proton in the ^1H NMR spectra of the diamagnetic Ni(II) and $\text{UO}_2(\text{II})$ complexes emphasizes the deprotonation of the enolized carbonyl oxygen ($=\text{C}-\text{O}^-$).

The most significant features of the ^{13}C NMR spectra of the Pd(II), Cd(II), Hg(II), Ni(II) and $\text{UO}_2(\text{II})$ complex were detected when comparing with the spectrum of the corresponding free ligand. From ^{13}C NMR spectral data, for the all diamagnetic complexes the signals for the C^8 carbon showed an downfield shift on complexation but the signals for the C^7 carbon showed an downfield shift in case of Ni(II) and $\text{UO}_2(\text{II})$ complexes where the same signal appears at upfield shift in case of Cd(II), Pd(II) and Hg(II) complexes [23] compared with the free ligand. Also, the appearance of new signals in $[\text{UO}_2(\text{L})(\text{OAc})(\text{H}_2\text{O})]$ complex at $\delta=172$

ppm and $\delta=52$ ppm give strong evidence for the presence of acetate group. The other ring carbon atoms did not show significant shifts.



Scheme 2: ¹H NMR Chemical shifts of (A) HL and (B) [Cd(HL)₂Cl₂] complex.



Scheme 3: ¹³C NMR Chemical shifts of (A) HL and (B) [Cd(HL)₂Cl₂] Complex

Electronic Spectra

The diamagnetic behaviour of $[\text{Ni}(\text{L})_2]$ complex indicates a square planar configuration. Further, the electronic spectrum shows a characteristic band at 18182 cm^{-1} assigned to ${}^1\text{A}_{1g} \rightarrow {}^1\text{A}_{2g}$ transition in a square planar geometry [24].

The copper (II) complex has magnetic value (1.98 B.M.), indicating the presence of Cu(II) ion. The electronic spectrum of $[\text{Cu}(\text{L})\text{Cl}]$ complex exhibits a broad band with a maximum at 14706 cm^{-1} , due to the ${}^2\text{B}_{1g} \rightarrow {}^2\text{A}_{1g}$ transition, as reported for square planar Cu(II) complex [25].

The electronic spectrum of $[\text{UO}_2(\text{L})(\text{OAc})(\text{H}_2\text{O})]$ complex shows two bands at 22222 and 27169 cm^{-1} may be attributed to ${}^1\text{E}_g \rightarrow {}^2\pi_u$ transition and charge transfer $n \rightarrow \pi^*$, respectively [26].

The diamagnetic $[\text{Pd}(\text{HL})_2\text{Cl}_2]$ complex [27] shows a band at 22624 cm^{-1} which is assigned to ${}^1\text{A}_{1g} \rightarrow {}^2\text{B}_{1g}$ transition in a square-planar configuration [28].

ESR studies

The solid-state ESR spectrum (Fig. 1) of $[\text{Cu}(\text{L})\text{Cl}]$ exhibits axially symmetric g-tensor parameters with g_{\parallel} (2.40) and g_{\perp} (2.09) > 2.0023 indicating that the copper site has a $d_{x^2-y^2}$ ground-state characteristic of tetrahedral, square planar or octahedral stereochemistry [29]. The spin-Hamiltonian parameters of this complex were calculated. In axial symmetry the g-values are related by the expression, $G = (g_{\parallel} - 2)/(g_{\perp} - 2) = 4$, where G is The exchange interaction parameter. According to Hathaway [30], if the value of G is greater than 4, the exchange interaction between Cu(II) centers in the solid state is negligible, whereas when is less than 4, a considerable exchange interaction is indicated in the solid complex. The calculated G value was 4.4 suggesting that there are no copper-copper exchange interactions.

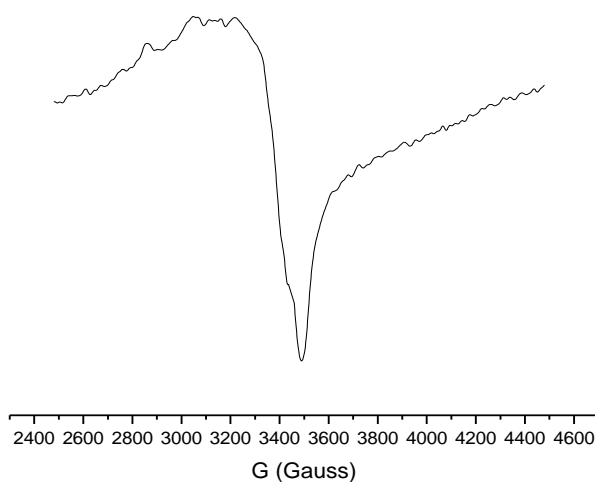


Fig 1: Room temperature solid state X-band ESR spectrum of $[\text{Cu}(\text{L})\text{Cl}]$ complex

The ability of A_{\parallel} ($180 \times 10^{-4} \text{ cm}^{-1}$) to decrease with increasing of g_{\parallel} is an evidence of an increase of the tetrahedral distortion in the coordination sphere of copper [31, 32]. In order to quantify the degree of distortion of the Cu(II) complexes, we selected the f factor $g_{\parallel}/A_{\parallel}$ obtained from the ESR spectra. Where, the f factor is regarded as an empirical index of tetrahedral distortion. Its value ranges between 105 and 135 for square planar complexes, depending on the nature of the coordinated atoms. In the presence of a tetrahedrally distorted structure the values can be much larger. For this complex, the $g_{\parallel}/A_{\parallel}$ quotient is 133, demonstrating the presence of significant dihedral angle distortion in the d_{xy} -plane and indicating a square-planar geometry. Superhyperfine structure for this complex was not seen at higher fields, excluding any interaction of the nuclear spins of nitrogen ($I = 1$) with the unpaired electron density on Cu(II) [33].

Molecular orbital coefficients, α^2 (covalent in-plane σ -bonding) and β^2 (covalent in-plane π -bonding) were calculated:

$$\alpha^2 = \left(\frac{A_{//}}{0.036} \right) + (g_{//} - 2.0023) + \frac{3(g_{\perp} - 2.0023)}{7} + 0.04$$

$$\beta^2 = \frac{(g_{//} - 2.0023)E}{-8\lambda\alpha^2}$$

$\lambda = 828 \text{ cm}^{-1}$ for the free ion and E is the ${}^2B_{1g} \rightarrow {}^2A_{1g}$ transition.

As a measure of the covalency of the in-plane σ -bonding $\alpha^2 = 1$ indicates complete ionic character, whereas $\alpha^2 = 0.5$ indicates 100% covalent bonding, with the assumption of negligibly small values of the overlap integral. The β^2 parameter gives an indication of the covalency of the in-plane π -bonding. The smaller β^2 , indicates the larger covalency of the bonding.

The value of α^2 (0.97) and β^2 (0.89) for the complex indicate that the in-plane σ -bonding and in-plane π -bonding are appreciably covalent and are consistent with very strong in-plane π -bonding in this complex. These results are anticipated because there are appropriate ligand orbitals to combine with the d_{xy} orbital of the Cu(II) ion. The higher value of α^2 compared with β^2 indicate that the in-plane π -bonding is more covalent than the in-plane σ -bonding. These data are highly consistent with other reported values.

Thermal Analysis

The TG-DTA results of the isolated complexes are listed in Table 1. The results show good agreement with the formulae suggested from the analytical data. The TG curves of the isolated complexes were taken as a proof for the existing of the coordinate chlorine atoms [34]. A general decomposition pattern was concluded in which the complexes decomposed in three steps. The complexes show thermal stability rather than the ligand where the beginning of its decomposition shifts to higher temperature (226–778 °C). In general, all complexes are thermally stable; [Ni(L)₂] complex is the highest one. It is thermally stable up to 307 °C above which point partial decomposition of the complex begins. In the temperature range 307–440 °C, the TG curve displays 58% weight loss which could be ascribed to the elimination of the two loosely bound (2C₆H₅+2C₅H₄N) fragments.

Table 1: Thermal behavior of metal complexes of HL

Complex (Mol.Wt.)	Temp. range (°C)	Decomp. prod. (formula wt.)	Wt. loss (%)	
			Found	Calcd
5 CuC ₁₄ H ₁₂ N ₃ OCl (337.33)	230-370	C ₆ H ₅ +½Cl ₂ (112.61)	33.5	33.4
	370-736	C ₈ H ₇ N ₃ (145.17)	43.1	43.0
	> 736	Residue, CuO (79.54)	23.4	23.6
6 PdC ₂₈ H ₂₆ N ₆ O ₂ Cl ₂ (655.96)	240-298	2C ₆ H ₅ +½Cl ₂ (225.93)	34.2	34.2
	298-720	2C ₈ H ₈ N ₃ +½O ₂ (308.35)	47.1	47.0
	> 720	Residue, PdO (74.929)	18.7	18.6
4 CdC ₂₈ H ₂₆ N ₆ O ₂ Cl ₂ (661.96)	226-383	2C ₆ H ₅ +½Cl ₂ (225.93)	34.1	34.0
	383-778	2C ₈ H ₈ N ₃ +½O ₂ (308.35)	46.7	46.6
	> 778	Residue, PdO (74.929)	18.7	18.6
2 NiC ₂₈ H ₂₄ N ₆ O ₂ (535.25)	307-440	2C ₆ H ₅ +2C ₅ H ₄ N (310.40)	58.0	57.9
	440-760	2C ₂ HN ₂ +½O ₂ (150.14)	27.9	28.1
	> 760	Residue, NiO (74.70)	14.1	14.0

The final weight loss of 27.9% ending at 760 °C, is attributed to complete decomposition of the remaining more tightly bound fragment of the organic molecule, alongside rupture of the chelate bond, leaving NiO comprising 14.1% of the initial mass of the complex.

Kinetic parameters

Coats–Redfern [35] and Horowitz–Metzger [36] are the two methods mentioned in the literature related to decomposition kinetics studies; these two methods are applied in this study.

From the TG curves, the activation energy, E_a , pre-exponential factor, A , entropies, ΔS^* , enthalpy, ΔH^* , and Gibbs free energy, ΔG^* , were calculated by well-known methods; where $\Delta H^* = E - RT$ and $\Delta G^* = \Delta H^* - T\Delta S^*$.

The linearization curves of Coats–Redfern and Horowitz–Metzger methods are shown in Figs. 2, 3. Kinetic parameters for the first stages, calculated by employing the Coats–Redfern and Horowitz–Metzger equations, are summarized in Tables 2, 3. The calculated values of E_a , ΔS^* , ΔH^* and ΔG^* for the decomposition steps are given in Tables 2, 3. According to the kinetic data obtained from DTG curves, the high values of the activation energies reflect the thermal stability of the complexes. The entropy of the activation was found to have negative values in all of the complexes. Negative values indicate that the decomposition reactions proceed with changes in order which may be more ordered due to the decomposition of the complexes. The positive sign of activation enthalpy change, ΔH^* indicates that the decomposition stages are endothermic processes. The positive sign of ΔG^* for the investigated complexes reveals that the free energy of the final residue is higher than that of the initial compound, and hence all the decomposition steps are non-spontaneous processes.

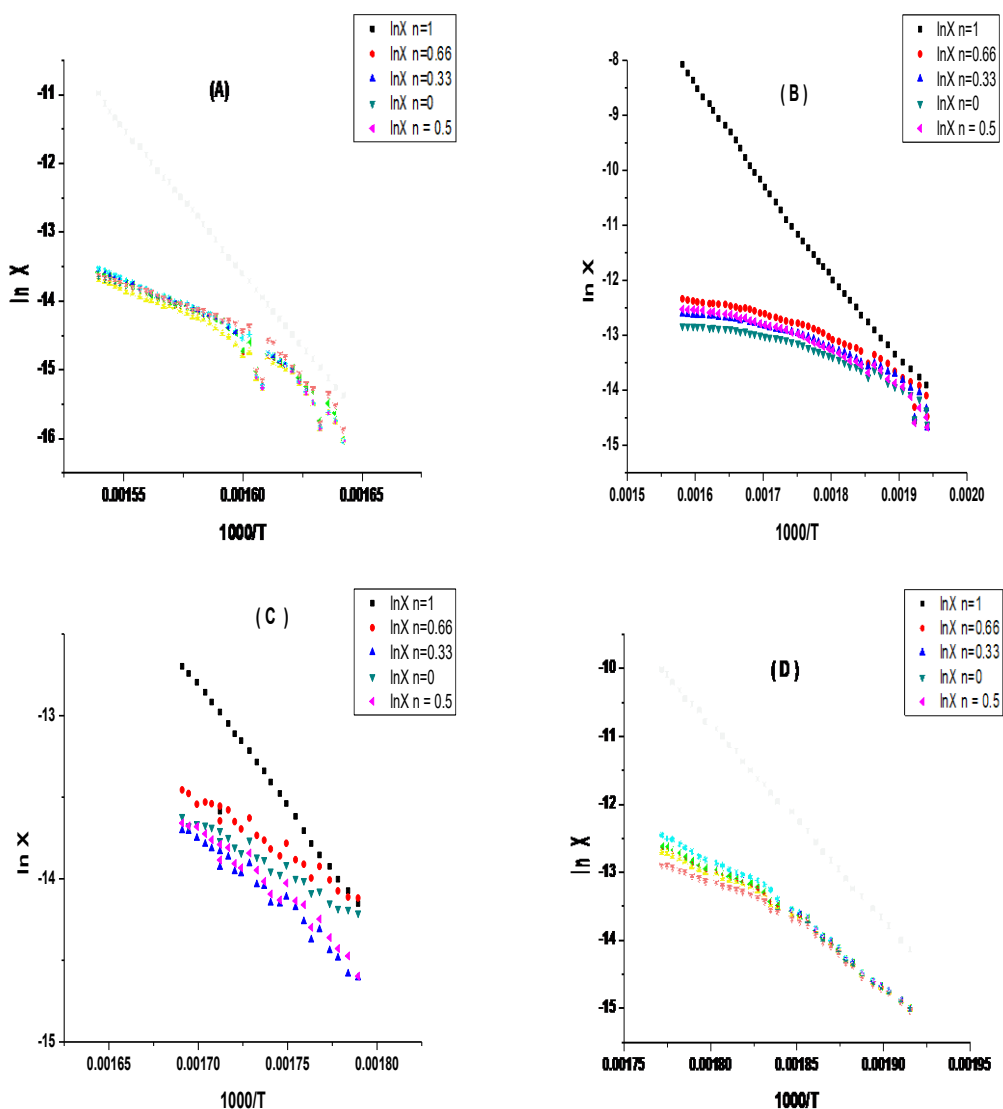


Fig 2: Coats-Redfern plots of (A) [Ni(L)₂], (B) [Cu(L)Cl], (C) [Cd(HL)₂Cl₂] and (D) [Pd(HL)₂Cl₂]

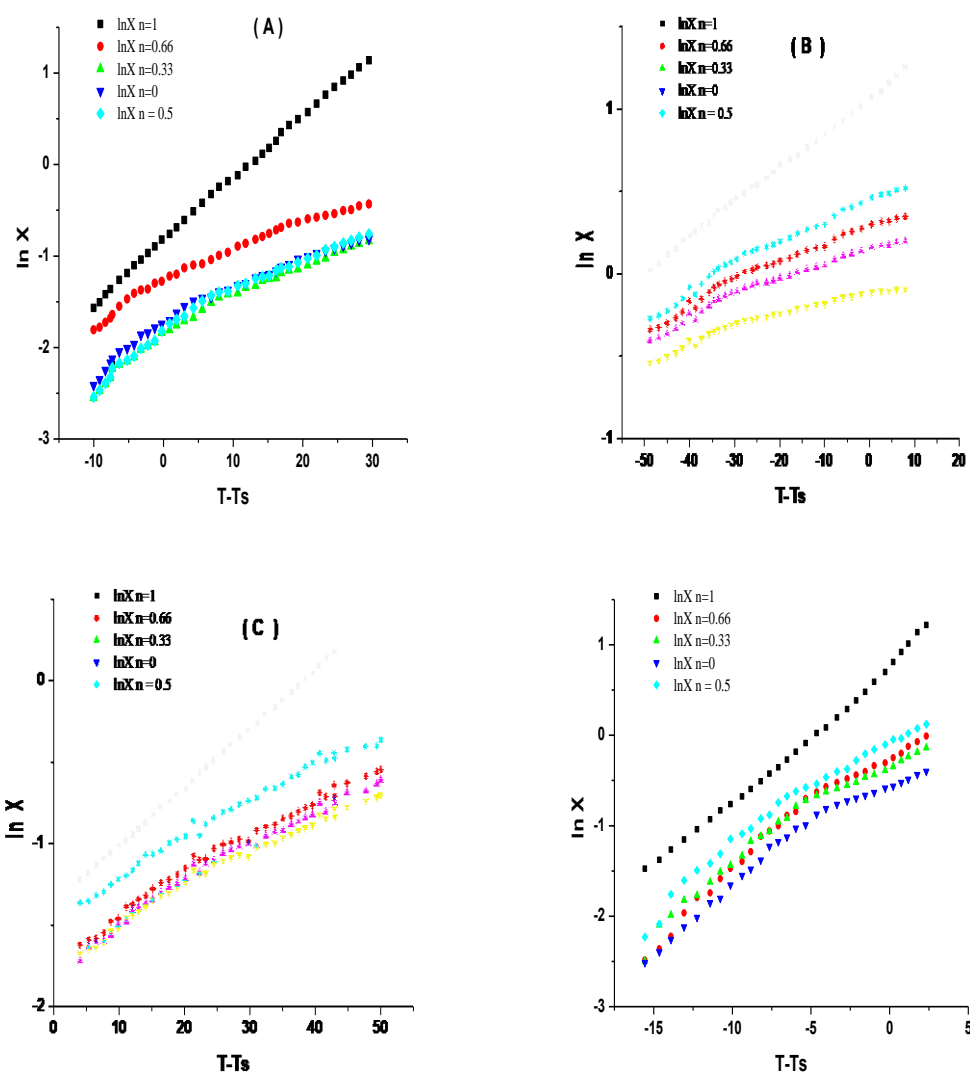

 Fig 3: Horowitz-Metzger plots of (A) $[Ni(L)_2]$, (B) $[Cu(L)Cl]$, (C) $[Cd(HL)_2Cl_2]$ and (D) $[Pd(HL)_2Cl_2]$

Table 2: Kinetic Parameters of complexes evaluated by Coats-Redfern equation

Complex	peak	Mid Temp(K)	Ea kJ/mol	A (S ⁻¹)	ΔH^* kJ/mol	ΔS^* kJ/mol.K	ΔG^* kJ/mol
2	1 st	624	546.69	8.20E-41	541.51	-0.1018	1177.02
	2 nd	872	873.24	2.29E-55	865.99	-0.1299	1999.43
5	1 st	572	113.88	7.21E-37	109.12	-0.9422	648.08
	2 nd	826	122.19	0.06834	115.33	-0.2757	343.05
4	1 st	551	219.40	1.38E-16	214.82	-0.5537	519.88
	2 nd	814	227.72	4.43E-7	13.70	-0.3749	318.86
6	1 st	542	433.72	1.13E-42	429.22	-0.1053	999.90
	2 nd	829	540.95	6.38E-4	534.06	-0.3146	794.85

Table 3: Kinetic Parameters of complexes evaluated by Horowitz-Metzger equation

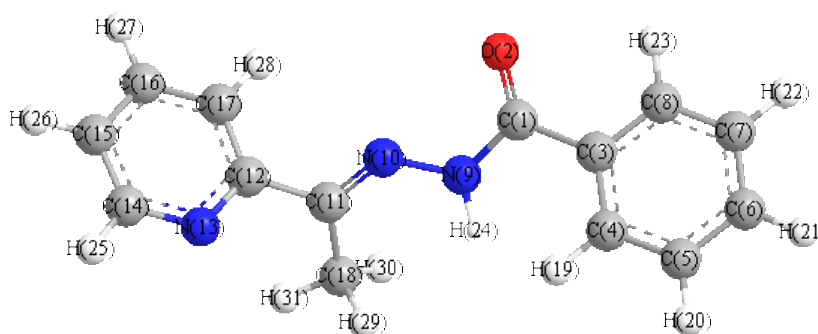
Complex	peak	Mid Temp(K)	Ea kJ/mol	A (S ⁻¹)	ΔH^* kJ/mol	ΔS^* kJ/mol.K	ΔG^* kJ/mol
2	1 st	624	546.58	7.74E-41	541.39	-0.1019	1177.21

5	2 nd	872	872.35	2.47E-55	865.09	-0.1299	1998.03
	1 st	572	112.61	7.41E-37	107.85	-0.9419	646.67
4	2 nd	826	122.47	0.08229	115.60	-0.2741	342.05
	1 st	551	227.07	1.36E-16	222.49	-0.5537	527.61
6	2 nd	814	20.22	4.71E-7	13.45	-0.3743	318.19
	1 st	542	434.86	1.12E-42	430.35	-0.1052	1001.07
	2 nd	829	33.94	4.09E-5	27.05	-0.3374	306.77

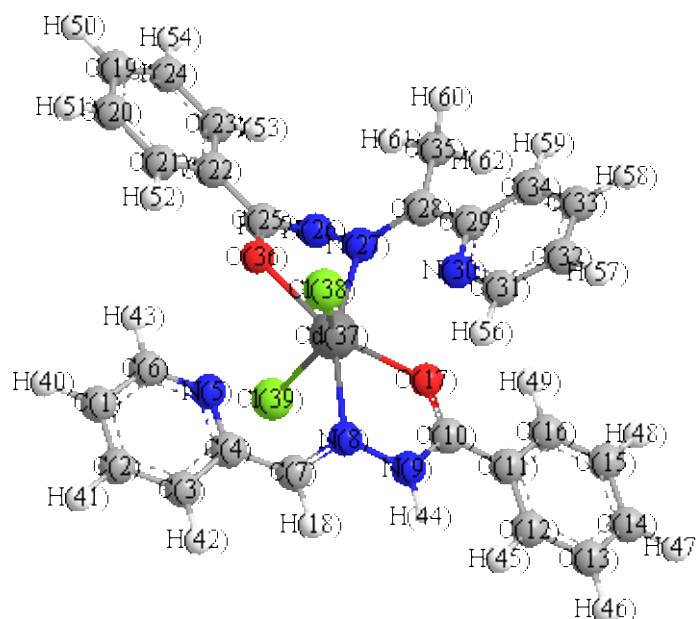
Molecular Modelling

An attempt to gain a better insight on the molecular structures of complexes **2**, **4**, **5** and **6** and the free ligand (E)-N`-(1-(pyridine-2-yl)ethylidene)benzohydrazide **1**, conformational analysis of the target compounds has been performed by MM+ [37] force field as implemented in HyperChem 8.03 [22]. The PM3 semiempirical [38] calculations performed on free ligand (E)-N`-(1-(pyridine-2-yl)ethylidene) benzohydrazide showed that the calculations performed indicate that the phenyl and pyridyl groups, showing highly free rotations, were spatially arranged itself approximately coplanar and perpendicular to the plane of core complex. Moreover, it is noteworthy to say that the MM+ and PM3 calculations give results which are in good agreement with the X-ray data of the structure analogues [39].

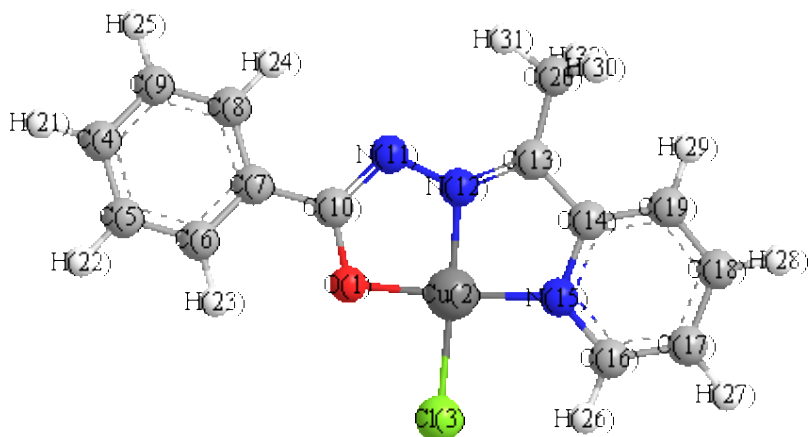
The molecular structure along with atom numbering of HL and its metal complexes are shown in structures (1 - 5). Analysis of the data in tables 1S - 10S (Supplementary Materials) calculated for the bond lengths and angles for the bond, one can conclude the following remarks:



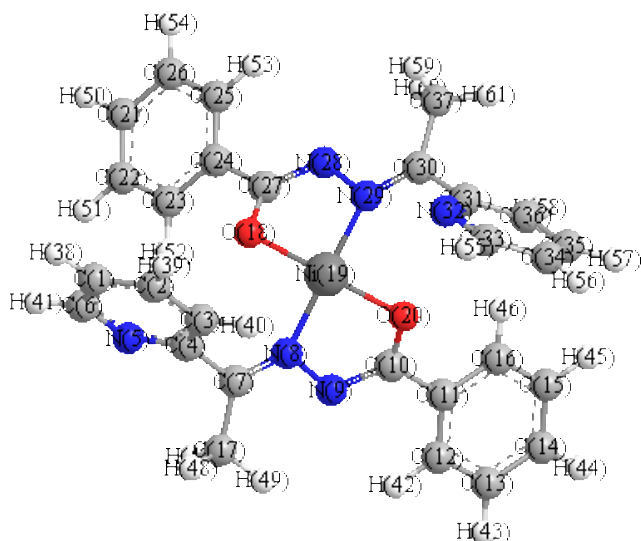
Structure 1: Molecular modeling of H₂L



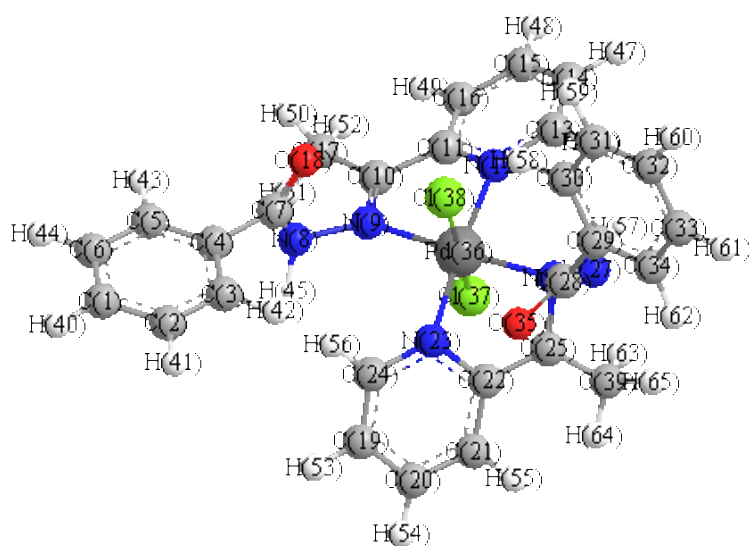
Structure 2: Molecular modeling of [Cd(HL)₂Cl₂] complex

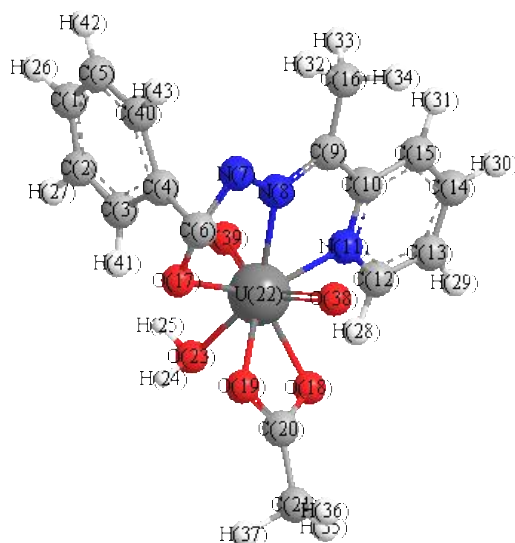


Structure 3: Molecular modeling of [Cu(L)Cl] complex



Structure 4: Molecular modeling of [Ni(L)₂] complex



Structure 5: Molecular modeling of [Pd(HL)₂Cl₂] complex

Structure 6: Molecular modeling of [UO₂(L)(OAc)(H₂O)] complex

1- The N(9)-N(10) bond length becomes slightly shorter in complexes as the coordination takes place via N atoms of -C=N-N=C- group that is formed on deprotonation of OH group in [Ni(L)₂], [Cu(L)Cl] and [Cd(HL)₂Cl₂] complexes.

2- The C(1)-O(2) bond distance in [Ni(L)₂], [Cu(L)Cl] and [Cd(HL)₂Cl₂] complexes becomes longer due to the formation of the M-O bond which makes the C-O bond weaker except [Pd(HL)₂Cl₂] complex in which this bond distance remains practically unaltered indicating that this group is not participated in bonding [40].

3- In [Ni(L)₂] and [Cu(L)Cl] complexes, C(1)-N(9) bond distance is more longer due to the deprotonation at O(18) which leads to a higher single bond character.

4- In [Ni(L)₂], [Cu(L)Cl] and [Cd(HL)₂Cl₂] complexes, C(1)-N(9) and N(10)-C(11) bond distances are shorten due to forming a double bond character.

5- The bond angles of the hydrazone moiety of HL are altered somewhat upon coordination but the angles around the metal undergo appreciable variations upon changing the metal center [41], the largest change affects C(11)-C(10)-N(9), C(1)-N(9)-N(10), N(10)-C(11)-C(12), and N(9)-C(1)-C(3) angles which are reduced or increased on complex formation as a consequence of bonding.

6- The bond angles in complexes namely, [Ni(L)₂] complex are quite near to a tetrahedral geometry predicting sp³ hybridization. On the other hand, [Cu(L)Cl] complex afforded a square planar geometry with dsp² hybridization. Also, [Cd(HL)₂Cl₂] and [Pd(HL)₂Cl₂] complexes afforded octahedral geometry.

7- The lower HOMO energy values show that molecules donating electron ability is the weaker. On contrary, the higher HOMO energy implies that the molecule is a good electron donor. LUMO energy represents the ability of a molecule receiving electron as in Table 4 [42].

Table 1S: Selected Bond length of H₂L

Bond	Length (Å)	Bond	Length (Å)
C(11)-C(12)	1.48	N(10)-C(11)	1.30
N(9)-N(10)	1.39	C(1)-N(9)	1.45
C(1)-C(3)	1.49	C(1)-O(2)	1.21

Table 2S: Selected Bond angles of H₂L

Angle	Degree(°)	Angle	Degree (°)
C(12)-C(11)-N(10)	115.95	C(11)-N(10)-N(9)	121.42
N(10)-N(9)-C(1)	116.63	N(9)-C(1)-C(3)	115.88

C(4)-C(3)-C(1)	121.22	N(9)-C(1)-O(2)	120.15
C(3)-C(1)-O(2)	123.78		

Table 3S: Selected Bond length of [Cd(HL)₂Cl₂]

Bond	Length (Å)	Bond	Length (Å)
Cd(37)-Cl(39)	2.47	Cd(37)-Cl(38)	2.48
O(36)-Cd(37)	2.10	N(27)-Cd(37)	2.17
C(28)-C(29)	1.35	N(27)-C(28)	1.35
N(26)-N(27)	1.36	C(25)-O(36)	1.21
C(25)-N(26)	1.44	C(22)-C(25)	1.36
O(17)-Cd(37)	2.11	C(10)-O(17)	1.21
N(9)-C(10)	1.38	C(10)-C(11)	1.36
N(8)-Cd(37)	2.16	N(8)-N(9)	1.35
C(7)-N(8)	1.34		

Table 4S: Selected Bond angles of [Cd(HL)₂Cl₂]

Angle	Degree(°)	Angle	Degree (°)
Cl(39)-Cd(37)-O(36)	85.67	Cl(38)-Cd(37)-O(36)	79.65
Cl(39)-Cd(37)-N(8)	84.04	Cl(38)-Cd(37)-N(27)	105.84
O(36)-Cd(37)-N(27)	61.94	N(27)-Cd(37)-O(17)	84.78
O(17)-Cd(37)-N(8)	72.89	C(29)-C(28)-N(27)	122.17
C(35)-C(28)-N(27)	118.04	Cd(37)-N(27)-C(28)	123.69
Cd(37)-N(27)-N(26)	116.35	C(28)-N(27)-N(26)	119.54
N(27)-N(26)-C(25)	86.20	O(36)-C(25)-N(26)	123.96
N(26)-C(25)-C(22)	119.96	O(36)-C(25)-C(22)	116.05
O(17)-C(10)-C(11)	121.71	O(17)-C(10)-N(9)	118.27
C(11)-C(10)-N(9)	120.01	C(10)-N(9)-N(8)	115.18
Cd(37)-N(8)-N(9)	112.88	Cd(37)-N(8)-C(7)	124.68
N(9)-N(8)-C(7)	122.36	N(8)-C(7)-C(4)	126.67

Table 5S: Selected Bond length of [Cu(L)Cl]

Bond	Length (Å)	Bond	Length (Å)
C(13)-C(14)	1.43	N(12)-C(13)	1.35
N(11)-N(12)	1.36	C(10)-N(11)	1.34
Cu(2)-N(15)	1.86	Cu(2)-N(12)	1.84
Cu(2)-Cl(3)	2.15	O(1)-C(10)	1.34

Table 6S: Selected Bond angles of [Cu(L)Cl]

Angle	Degree(°)	Angle	Degree (°)
C(16)-N(15)-Cu(2)	131.80	C(14)-N(15)-Cu(2)	109.02
C(14)-C(13)-N(12)	111.89	C(13)-N(12)-N(11)	132.92
C(7)-C(10)-O(1)	117.18	N(11)-C(10)-O(1)	121.41
N(11)-C(10)-C(7)	121.40	N(12)-N(11)-C(10)	112.26
N(11)-N(12)-Cu(2)	110.42	C(13)-N(12)-Cu(2)	114.48
N(15)-Cu(2)-N(12)	87.61	N(15)-Cu(2)-Cl(3)	93.91
N(12)-Cu(2)-O(1)	88.79	Cl(3)-Cu(2)-O(1)	89.77

Table 7S: Selected Bond length of [Ni(L)₂]

Bond	Length (Å)	Bond	Length (Å)
C(30)-C(31)	1.48	N(29)-C(30)	1.31

N(28)-N(29)	1.39	C(27)-N(28)	1.34
C(10)-O(20)	1.32	C(10)-C(11)	1.47
N(9)-C(10)	1.34	N(8)-Ni(19)	1.85
N(8)-N(9)	1.40	C(7)-N(8)	1.31

 Table 8S: Selected Bond angles of [Ni(L)₂]

Angle	Degree(°)	Angle	Degree(°)
C(37)-C(30)-N(29)29	123.74	C(31)-C(30)-N(29)	121.93
C(30)-N(29)-N(28)	118.76	N(28)-C(27)-C(24)	121.36
N(29)-N(28)-C(27)	114.36	N(28)-C(27)-O(18)	119.45
C(24)-C(27)-O(18)	119.10	O(18)-Ni(19)-N(8)	91.59
N(29)-Ni(19)-O(20)	91.54	N(29)-Ni(19)-O(18)	88.58
O(20)-Ni(19)-N(8)	88.11	O(20)-C(10)-N(9)	119.10
O(20)-C(10)-C(11)	119.11	C(11)-C(10)-N(9)	121.67
C(11)-C(10)-N(9)	121.67	C(10)-N(9)-N(8)	114.18
N(9)-N(8)-C(7)	119.09	N(8)-C(7)-C(4)	121.61

 Table 9S: Selected Bond length of [Pd(HL)₂Cl₂]

Bond	Length (Å)	Bond	Length (Å)
Pd(36)-Cl(38)	2.32	Pd(36)-Cl(37)	2.34
C(28)-O(35)	1.21	C(28)-C(29)	1.49
N(27)-C(28)	1.43	N(26)-Pd(36)	1.97
N(26)-N(27)	1.50	C(25)-N(26)	1.44
N(23)-Pd(36)	1.97	C(7)-N(8)	1.45
N(12)-Pd(36)	1.98	N(9)-Pd(36)	2.00
C(10)-C(11)	1.48	N(9)-C(10)	1.32
N(8)-N(9)	1.49	C(7)-O(18)	1.21

 Table 10S: Selected Bond angles of [Pd(HL)₂Cl₂]

Angle	Degree(°)	Angle	Degree(°)
Cl(38)-Pd(36)-N(26)	92.26	Cl(38)-Pd(36)-N(12)	90.99
Cl(37)-Pd(36)-N(23)	93.05	N(26)-Pd(36)-N(23)	86.85
Cl(37)-Pd(36)-N(9)	82.65	N(26)-Pd(36)-N(12)	89.47
N(23)-Pd(36)-N(9)	97.25	N(12)-Pd(36)-N(9)	86.17
O(35)-C(28)-C(29)	123.62	O(35)-C(28)-N(27)	121.08
C(29)-C(28)-N(27)	115.12	C(28)-N(27)-N(26)	122.94
N(27)-N(26)-C(25)	112.58	C(39)-C(25)-N(26)	117.77
C(17)-C(10)-C(11)	118.75	C(17)-C(10)-N(9)	124.44
C(39)-C(25)-C(22)	123.47	N(26)-C(25)-C(22)	118.66
C(11)-C(10)-N(9)	116.62	C(10)-N(9)-N(8)	115.17
N(9)-N(8)-C(7)	111.09	O(18)-C(7)-N(8)	117.35
O(18)-C(7)-C(4)	126.52	N(8)-C(7)-C(4)	115.96

 Table 11S: Selected Bond length of [UO₂(L)(OAc)(H₂O)]

Bond	Length (Å)	Bond	Length (Å)
U(22)-O(39)	1.99	U(22)-O(38)	1.99
U(22)-O(23)	2.10	O(19)-U(22)	2.09
O(18)-U(22)	2.07	O(17)-U(22)	2.08
N(11)-U(22)	2.13	N(8)-C(9)	1.34
C(9)-C(10)	1.34	N(8)-U(22)	2.13
N(7)-N(8)	1.38	C(6)-O(17)	1.34

Table 12S: Selected Bond angles of [UO₂(L)(OAc)(H₂O)]

Angle	Degree(°)	Angle	Degree (°)
O(39)-U(22)-O(17)	101.48	O(39)-U(22)-N(11)	69.66
O(39)-U(22)-N(8)	81.01	O(38)-U(22)-O(18)	75.74
O(38)-U(22)-N(11)	78.54	O(23)-U(22)-O(19)	72.47
O(23)-U(22)-O(17)	87.93	O(19)-U(22)-O(18)	55.53
O(18)-U(22)-N(11)	85.51	O(17)-U(22)-N(8)	76.42
N(11)-U(22)-N(8)	70.75	C(10)-C(9)-N(8)	113.51
C(9)-N(8)-N(7)	125.26	N(8)-N(7)-C(6)	107.16
O(17)-C(6)-N(7)	125.77		

Table 4: The molecular parameters of the ligand and its complexes

The assignment of the theoretical parameters	The compound investigated	The theoretical data
Total Energy	1	= -60822.1881475 (kcal/mol)
Total Energy		= -96.926314499 (a.u.)
Binding Energy		= -3415.2186145 (kcal/mol)
Isolated Atomic Energy		= -57406.9695330 (kcal/mol)
Electronic Energy		= -387305.9216624 (kcal/mol)
Core-Core Interaction		= 326483.7335149 (kcal/mol)
Heat of Formation		= 53.1263855 (kcal/mol)
Dipole moment		= 2.80 (Debys)
Homo		= -9.39
Lumo		= -0.47
Total Energy	2	= -145061.4150843 (kcal/mol)
Total Energy		= -231.170051069 (a.u.)
Binding Energy		= -7052.8375233 (kcal/mol)
Isolated Atomic Energy		= -138008.5775610 (kcal/mol)
Electronic Energy		= -1351493.4443371 (kcal/mol)
Core-Core Interaction		= 1206432.0292528 (kcal/mol)
Heat of Formation		= -117.5515233 (kcal/mol)
Dipole moment		= 2.09 (Debys)
Homo		= -9.05
Lumo		= -0.66
Total Energy	5	= -95136.6011485 (kcal/mol)
Total Energy		= -151.609805635 (a.u.)
Binding Energy		= -3554.4287875 (kcal/mol)
Isolated Atomic Energy		= -91582.1723610 (kcal/m
Electronic Energy		= -563487.5195679 (kcal/mol)
Core-Core Interaction		= 468350.9184194 (kcal/mol)
Heat of Formation		= -28.4957875 (kcal/mol)
Dipole moment		= 4.35 (Debys)
Homo		= -4.61
Lumo		= -0.81
Total Energy	6	= -160525.0064044 (kcal/mol)
Total Energy		= -255.812849384 (a.u.)
Binding Energy		= -7271.2168414 (kcal/mol)
Isolated Atomic Energy		= -153253.7895630 (kcal/mol)
Electronic Energy		= -1580150.0880841 (kcal/mol)
Core-Core Interaction		= 1419625.0816797 (kcal/mol)
Heat of Formation		= -186.5468414 (kcal/mol)
Dipole moment		= 10.14 (Debys)

Homo	= - 6.37
Lumo	= - 1.99

Biological activity

Antimicrobial activity

The tested microorganisms were obtained from the culture collection at the Microbiology laboratory, National Organization for Drug Control and Research (NODCAR). All synthesized target compounds were evaluated for their in vitro antibacterial activity against the gram-positive *B. subtilis*, *S. aureus* and the Gram-negative *P. aeruginosa*, *Escherichia coli*. They were also evaluated for their in vitro antifungal and pathogenic fungi *A. niger*, *Candida albicans*.

Minimum inhibitory concentration (MIC) [43, 44] was determined for each of the active compounds along with Gentamycin and Colitrimazole as standard controls; results are shown in Table 5. This screening was performed against the gram-positive *B. subtilis*, *S. aureus*, and gram-negative bacteria *P. aeruginosa*, *Escherichia coli* and pathogenic fungi *A. niger*, *Candida albicans*. The tested compounds were dissolved in dimethylsulfoxide (DMSO) at a concentration of 1 mg/ml. amongst all the compounds tested, **4** and **5** demonstrated the most potent antimicrobial and antifungal activity. It is noteworthy that the observed antimicrobial activity was highly dependent on the metal complex, in which copper complex played an important role in achieving an excellent level of biological activity. It is observed from these studies that most of the metal chelates have a higher activity than the free ligand. Such increased activity of the metal chelates can be explained on the basis of Overtone's concept and chelation theory [53]. According to Overtone's concept of cell permeability the lipid membrane that surrounds the cell favours the passage of only lipid soluble materials due to which liposolubility is an important factor that controls antimicrobial activity. On chelation, the polarity of the metal ion is reduced to a greater extent due to the overlap of the ligand orbital and partial sharing of the positive charge of the metal ion with donor groups. Further, it increases the delocalization of p-electrons over the whole chelate ring and enhances the lipophilicity of the complex. This increased lipophilicity enhances the penetration of the complexes into lipid membranes and blocking of metal binding sites on the enzymes of the microorganism. It was observed from the Table 5, complexes demonstrated the lowest potent antimicrobial activity.

Table 5: Antimicrobial and antifungal activities in terms of MIC (µg/ml) after 48h

Compound	<i>B. subtilis</i>	<i>S. aureus</i>	<i>P. aeruginosa</i>	<i>E. coli</i>	<i>A. niger</i>	<i>C. albicans</i>
1	1250	650	850	750	1000	750
2	750	450	1200	1500	875	750
3	900	600	2000	3000	550	375
4	300	145	112	46.87	8.5	1.87
5	350	140	144	46.87	5.25	3.75
6	650	925	550	750	550	375
7	850	750	2500	1500	1250	1500
Gentamycin	375	150	175	375	-	-
Colitrimazole	-	-	-	-	6.75	5.85

Table 6: In vitro cytotoxicity of HL and its metal complexes (Ehrlich ascites cells dead %)

Compound	IC50 (mg/mL)	% Dead		
		ED100 µl	ED50 µl	ED25 µl
5FU	1.5	95	61.1	38.2
1	1.8	92	58	35.5
2	1.6	95	62.2	37.5

Compound	IC ₅₀ (mg/mL)	% Dead		
		ED100 μ l	ED50 μ l	ED25 μ l
3	1.4	96.7	75.9	47.6
4	1.2	100	95.1	86
5	1.8	86.1	41.3	23.1
6	1.3	98.3	74	48
7	1.7	90	57.6	36.8

Tested compounds were prepared (1 mg/mL) in 100 mL DMSO and complete to 1 mL using RPMI-1640 medium. 5-Flourouracil (25 mg/mL) in 100 mL DMSO and complete to 1 mL using RPMI-1640 medium. Where, ED100, ED50, and ED25 are the effective doses at 25, 50, and 100 μ l, respectively, of the compounds used. The dead % refers to the % of the dead tumor cells and 5FU is 5-flourouracil as a well known cytotoxic agent.

Effect of drugs on the viability of Ehrlich ascites cells in vitro

(HL) and its Ni(II), Cu(II), Pd(II), Cd(II), Hg(II) and UO₂(II) complexes were tested for cytotoxicity against EAC in vitro. EAC cells were used because they have a very well known established model [46]. Results for the ED100, ED50 and ED25 values of the active compounds are summarized in Table 6. Comparisons of these cytotoxic activity values the standard drug 5-FU with those of complexes revealed that the compound **2** has shown nearly the same cytotoxic activity produced by the standard drug 5-FU. For compounds **3**, **4** and **6** were the most potent using ED100, ED50 and ED25 even higher than that of 5-FU. The rest of compounds showed less activity than standard drug 5-FU. Therefore, these compounds 2, 3, 4 and 6 can be used as a promising anti-tumor agent in vivo to inhibit the DNA replication in the cancer cells and not allow the tumor for further growth.

Antioxidant activity

Since the main mechanism of antioxidant action in foods is radical-scavenging, many methods have been developed in which the antioxidant activity is evaluated by the scavenging of synthetic radicals in polar organic solvents such as methanol at room temperature. The 2,2'-diphenyl-1-picrylhydrazyl (DPPH) radical assay provides an easy and rapid way to evaluate the antiradical activities of antioxidants (AH). Determination of the reaction kinetic types DPPH is a product of the reaction between DPPH• and an antioxidant:



The reversibility of the reaction is evaluated by adding DPPHH at the end of the reaction. If there is an increase in the percentage of remaining DPPH• at the plateau, the reaction is reversible, otherwise it is a complete reaction.

DPPH was used as stable free radical electron acceptor or hydrogen radical to become a stable diamagnetic molecule [47]. DPPH is a stable free radical containing an odd electron in its structure and usually used for detection of the radical scavenging activity in chemical analysis [48]. The DPPH method was carried out in a homogeneous phase and has the advantage of establish a real ranking hierarchy of antioxidant activity of electron- or H-donating agents, since it was not affected by some factors, which interfere in other model systems, such as metal chelation or partitioning abilities [49,50]. The reduction capability of DPPH radicals was determined by decrease in its absorbance at 517 nm induced by antioxidants [51].

We found that most of the compounds showed considerable free radical-scavenging activities (Table 7). Compound **6** was the strongest radical scavenger among fungal isolates with IC₅₀ 8.03 mg/mL, followed by compound **5** with IC₅₀ 10.05 mg/mL followed by compound **4** with IC₅₀ 12.23 mg/mL then compound **2** with IC₅₀ 15.2 mg/mL while compound **4** with IC₅₀ 16.24 mg/mL. However, the other compounds were moderate radical scavengers with IC₅₀ with IC₅₀ 38.78 and 49.56 mg/mL.

Table 7: DPPH inhibition of chemical compounds

Chemical compounds	DPPH IC ₅₀ (mg/mL)
Ascorbic acid	0.39
1	8.24
2	7.20
3	30.78
4	5.23
5	3.05
6	1.03
7	44.56

Table 8: Hemolytic activity of HL and its metal complexes

Chemical compounds	Absorbance (A)	% Erythrocyte hemolysis A/B X 100
Dist-H ₂ O (Abs.B)	0.967	100%
Vit-C	0.011	1.13
1	0.013	1.34
2	0.012	1.24
3	0.027	2.79
4	0.015	1.55
5	0.011	1.13
6	0.010	1.02
7	0.034	3.51

Hemolysis Activity

All the compounds were tested for hemolytic activity against red cells as shown in (Table 8). The compounds **6** and **5** show less hemolytic activity while other compounds show moderate to high hemolytic activity. The results are very interesting and much helpful for drug designing.

CONCLUSIONS

In this paper, (E)-N¹-(1-(pyridine-2-yl)ethylidene)benzohydrazide (HL) and its Ni(II), Cu(II), Pd(II), Cd(II), Hg(II) and UO₂(II) complexes were synthesized and characterized. It is interesting that some complexes have various biological activities. Compounds **4** and **5** have antibacterial and antifungal activities, compounds **2**, **3**, **4** and **6** have antitumor activities while compound **6** has antioxidant activity.

REFERENCES

- A. Alama, B. Tasso, F. Novelli, F. Sparatore, *Drug Discov. Today* 14 (2009) 500–508 [1]
 A. Levina, A. Mitra, P.A. Lay, *Metallomics* 1 (2009) 458–470. [2]
 E.S. Antonarakis, A. Emadi, *Pharmacol.* 66 (2010) 1–9. [3]
 R.R. Zaky, K.M. Ibrahim, I.M. Gabr, *Spectrochim. Acta A* 81 (2011) 28–34. [4]
 R.R. Zaky, T.A. Yousef, *J. Mol. Struct.* 1002 (2011) 76–85. [5]
 K. M. Ibrahim, I.M. Gabr, G.M. Abu El-Reash, R.R. Zaky, *Monatsh. Fur Chem.* 140(6) (2009) 625–632. [6]
 M.L. Bolognesi, R. Budriesi, A. Cavalli, A. Chiarini, R. Gotti, A. Leonardi, A. Minarini, E. Poggesi, M. Recanatini, M. Rosini, V. Tummiatti, C. Melchiorre, *J. Med. Chem.* 42 (1999) 4214–4224. [7]
 I. Cantuti-Castelvetri, B. Shukitt-Hale, J.A. Joseph, *Int. J. Dev. Neurosci.* 18 (2000) 367–381. [8]
 J. Vaya, M. Aviram, *Curr. Med. Chem.-Immunol. Endocr. Metab. Agents* 1 (2001) 99–117. [9]
 O. Blokhina, E. Virolainen, K.V. Fagerstedt, *Ann. Bot.* 91 (2003) 179–194. [10]
 P.C.H. Hollman, M.B. Katan, *Food Chem. Toxicol.* 37 (1999) 937–942. [11]
 T.A. Yousef, F.A. Badria, S.E. Ghazy, O.A. El-Gammal, G.M. Abu El-Reash *Int. J. Med. Med. Sci.* 3(2) (2011) 37–46. [12]

- R. R. Zaky, A. M. Abdelghay, *Research J. Pharmaceutical, Biological and Chemical Sciences* 2(1) (2011) 757–764. [13]
- T. A. Yousef, T. H. Rakha, U. El-Ayaan, G. M. Abu El-Reash, *J. Mol. Struct.* 1007 (2012) 146–157. [14]
- K.K. Narang, V.P. Singh, *Transit. Met. Chem.* 21 (1996) 507–511. [15]
- T.A. Yousef, O.A. El-Gammal, S.E. Ghazy, G.M. Abu El-Reash, *J. Mol. Struct.* 1004 (2011) 271–283. [16]
- T. A. Yousef, G. M. Abu El-Reash, T. H. Rakha, Usama El-Ayaan, *Spectrochim. Acta A* 83 (2011) 271–278. [17]
- R.J. Butcher, J. Jasinski, G.M. Mockler, E. Sinn, *J. Chem. Soc. Dalton. Trans.* (1976) 1099–1102. [18]
- G.A.A. AL-Hazmiy, M.S. EL-Shahawiz, I.M. Gabr, A.A. EL-Asmy, *Coord. Chem.* 58 (2005) 713–733. [19]
- S.P. McGlynn, J.K. Smith, *J. Chem. Phys.*, 35 (1961) 105–116. [20]
- L.H. Jones, *J. Opt. Soc. Am.* 54 (1964) 1283–1284. [21]
- HyperChem version 8.0 Hypercube, Inc [22]
- M.V. Angelusiu, S.F. Barbuceanu, C. Draghici, G.L. Almajan, *Europ. J. Med. Chem.* 45 (2010) 2055–2062. [23]
- K.M. Ibrahim, I.M. Gabr, R.R. Zaky, *J. Coord. Chem.*, 62(7) (2009) 1100–1116. [24]
- A.B.P. Lever, “*Inorganic Electronic Spectroscopy*, 2nd edn.”, Elsevier, Amsterdam (1984). [25]
- R.R. Zaky, *Phosphorus Sulfur Silicon Relat. Elem.* 186(2) (2011) 365–380. [26]
- K.M. Ibrahim, R.R. Zaky, E.A. Gomaa, M.N. El-Hady, *Research Journal of Pharmaceutical, Biological and Chemical* 2(3) (2011) 391–404. [27]
- A.A. El-Asmy, M.M. Hassanian, M.H. Abdel-Rhman, *J. Sulfu. Chem.* 31(2) (2010) 141–151. [28]
- P. Bindu, M.R.P. Kurup, T.R. Satyakeerty, *Polyhedron* 18 (1999) 321–331. [29]
- B.J. Hathaway, D.E. Billing, *Coord. Chem. Rev.* 5 (1970) 143–207. [30]
- J.L. Mesa, M.I. Pizarro, *Cryst. Res. Technol.* 33 (1998) 489–495. [31]
- O.I. Singh, M. Damayanti, N.R. Singh, R.K.H. Singh, M. Mohapatra, R.M. Kadam, *Polyhedron* 24 (2005) 909–916. [32]
- K.K. Narang, V.P. Singh, *Transit. Met. Chem.* 21 (1996) 507–511. [33]
- T.H. Rakha, K.M. Ibrahim, M.E. Khalifa, *Thermochim. Acta* 144 (1989) 53–63. [34]
- A.W. Coats, J.P. Redfern, *Nature* 20(1964) 68–69. [35]
- H.H. Horowitz, G. Metzger, *Anal. Chem.* 25(1963) 1464–1468. [36]
- N.L. Allinger, *J. Am. Chem. Soc.* 99 (1977) 8127–8134. [37]
- J.J.P. Stewart, *J. Comput. Chem.* 2 (1989) 209–220. [38]
- Jun Xu*, You-Qin Shu and Ping Hu Z. *Kristallogr. NCS* 226 (2011) 63–64 / DOI 10.1524/ncrs.2011.0031 [39]
- A.A.R. Despaigne, J.G. da Silva, A.C.M. do Carmo, O.E. Piro, E.E. Castella, H. Beraldo, *J. Mol. Struct.* 920 (2009) 97–102. [40]
- A.A.R. Despaigne, J.G. da Silva, A.C.M. do Carmo, F. Sives, O.E. Piro, E.E. Castellano, H. Beraldo, *Polyhedron* 28 (2009) 3797–3803. [41]
- S. Sagdinc, B. Koksoy, F. Kandemirli, S.H. Bayari, *J. Mol Struct.* 917 (2009) 63–70. [42]
- P.R. Murray, E.J. Baron, M.A. Pfaller, F.C. Tenover, R.H. Tenover, in: G.L. Wood, J. A. Washington (Eds.), *Manual of Clinical Microbiology*, Am. Soc. Microbiol., Washington, DC, 1995. [43]
- R.N. Jones, A.L. Barry, T.L. Gavan, I.I.J.A. Washington, in: E.H. Lennette, A. Ballows, W.J. Hausler Jr, H.J. Shadomy (Eds.), *Manual of Clinical Microbiology*, fourth edn, Am. Soc. Microbiol. (1972), Washington DC, 1985. [44]
- N. Raman, V. Muthuraj, S. Ravichandran, A. Kulandaisamy, *Proc. Indian Acad. Sci.* 115 (2003) 161–167. [45]
- K. Karrer, J.R. Rtjbini, *Pharmacology* 13 (1965) 124–130. [46]
- P.D. Duh, Y.Y. Tu, G.C. Yen, *Lebn. Wissen. Technol.* 32 (1999) 269–277. [47]
- B. Matthaus, *J. Agric. Food Chem.* 50 (2002) 3444–3452. [48]
- F.A.M. Silva, F. Borges, C. Guimaraes, J.L.F.C. Lima, C. Matos, S. Reis, *J. Agric. Food Chem.* 48 (2000) 2122–2126. [49]
- C. Siquet, F. Paiva-Martins, J.L.F.C. Lima, S. Reis, F. Borges, *Free Radical. Res.* 40 (2006) 433–442. [50]
- S.B. Bukhari, S. Memon, M. Mahroof-Tahir, M.I. Bhangar, *Spectrochim. Acta Part A* 71 (2009) 1901–1906. [51]
- A.I. Vogel, “*Vogel’s text book of quantitative chemical analysis*, 5th edn.”, Longmans, Amsterdam (1989). [52]
- I. Stylianakis, A. Kolocouris, N. Kolocouris, G. Fytas, G.B. Foscolos, E. Padalko, J. Neyts, D. Clerq, E. Bioorg, *Med. Chem. Lett.* 13 (2003) 1699–1703. [53]
- K.R. Sheeja, G. Kuttan, R. Kuttan, *Amala Res. Bull.* 17 (1997) 73–76. [54]
- J. Sambrook, E.F. Fritsh, T. Maniatis, *Molecular Cloning: A Laboratory Manual*, Cold Spring Harbor Laboratory Press, Cold Spring Harbor, NY (1989). [55]
- M. Cuendet, K. Hostettmann, O. Potterat, *Helv. Chim. Acta* 80 (1997) 1144–1152. [56]
- M. Burits, F. Bucar, *Phytother. Res.* 14 (2000) 323–328 [57]